COMMUNICATIONS IN SCIENCE AND TECHNOLOGY
Homepage: cst.kipmi.or.id

Statistical characteristics of time series temperature in cooling the electric vehicle controller using the bubble generator

IGNB. Catrawedarma*, Anggra Fiveriati, Abdul Hamid

Department of Mechanical Engineering, Politeknik Negeri Banyuwangi, Banyuwangi 68461, Indonesia

Article history:
Received: 9 December 2025 / Received in revised form: 15 May 2026 / Accepted: 30 May 2026

Abstract

The present study examines the thermal performance of the cooling system in an electric vehicle controller. This is achieved by injecting bubbles into the water block at various input airflow rates, using quiet-water and circulating-water cooling fluids. The thermal performance of a system is determined by two factors: the maximum temperature at the controller-water block interface and the corresponding thermal resistance. The temperature distribution is analyzed using statistical moments, the Probability Density Function (PDF), and Kolmogorov entropy to determine the irregularity of the temperature signal. The findings indicate that an increase in airflow rate can result in a decrease in maximum temperature and an enhancement in thermal resistance and flatness of the PDF curve. The maximum temperature decreases by 15.5% when the cooling medium is quiet water when compared to bubble injection at an airflow rate of Qa = 1.5 lpm. The bubble-cooling fluid, with an airflow rate of Qa = 1.5 lpm has a relatively uniform entropy across all thermocouple positions. The presence of low Kolmogorov entropy and low PDF flatness indicate a more stable controller response and fewer extreme spikes. In turn, it has an impact on the increasing system reliability and extending the durability of the controller's electronic components.

Keywords: Water block; thermal resistance; kolmogorov entropy

1. Introduction

Controller is a critical component in electric vehicles that regulates electrical power from the battery to the drive motor. The generation of heat is a result of continuous operation for a long time or under excessive load. It is then imperative that a cooling system is implemented to maintain the controller's optimal temperature below 175 °C. This is critical to ensure operation and preventing the risk of performance degradation, premature damage, and fire hazards [1,2]. It is important to note that the ability of the controller to execute its function of power regulation is dependent upon the maintenance of a controlled temperature. Maintaining an optimal temperature is instrumental in preventing premature damage and extending the lifespan of controller. The cooling system also prevents the controller from overheating, which can pose a hazard not only to the driver but also to the vehicle itself.

Conventional cooling methods applied to both batteries and electric vehicle controllers include air cooling, both natural and forced convection. Air cooling methods are simple to produce and maintain, but they are less efficient due to their low heat transfer coefficient [3]. The design and maintenance of air-cooling methods are more difficult and require external power to operate [1,2,4]. However, water has a higher heat transfer coefficient than air, allowing it to absorb more heat [5].

The cooling method that employs phase change material (PCM) utilizes the large latent heat of the medium that undergoes a phase change from solid to liquid state to absorb heat [1,6–10], [11–13]. However, PCM has high heat accumulation and low thermal conductivity. Consequently, it is pivotal to combine it with high-thermal-conductivity materials including copper foam and nickel [13,14], graphene [15], graphite [16,17], and silica [18]. The selection of PCM material is dependent upon its melting point, which must be exceed the operating temperature of the battery or controller [19].

The combination of PCM with a heat pipe is an alternative means of increasing the rate of heat dissipation. Heat pipes are included in the compact device category, and their complex manufacturing process makes them difficult to produce. The system is comprised of three zones: evaporation, adiabatic, and condensation. However, this method is more flexible because the geometry can be adjusted to the device to be used and does not require external power [20]. To enhance efficiency and effectiveness, a combination of heat pipe cooling systems with air and liquid cooling systems has been adopted [21]. To enhance the temperature distribution on the battery surface and the heat transfer area from its surface to the cooling pipe-based

* Corresponding author. Tel.: +6281229392829
Email: ignb.catrawedarma@poliwangi.ac.id
https://doi.org/10.21924/cst.11.1.2026.1858

heat sink, it is important to increase the thermal contact area between the battery and the cooling heat pipe [6,22,23]. Thermoelectric generators have been demonstrated to be effective in the cooling of batteries and controllers through the conversion of heat into electricity in view of the Seebeck effect [19].

Immersion cooling systems are categorized into three different classification: partially and fully immersed forced-flow systems and static cooling system. Immersion cooling employs a dielectric fluid with a higher thermal conductivity than air to absorb heat. This technique has been demonstrated to inhibit thermal runaway and reduce thermal resistance [24]. Immersion cooling has been observed to cause high-flow energy losses when utilizing high-viscosity fluids. To encounter these losses, high-power pumps are required. The issue of energy density is one of the most significant challenges for immersion cooling systems [24].

It is essential to considere the implementation of an alternative cooling method through the injection of air bubbles into the cooling channels. To date, the application of bubble cooling has only been utilized in heat exchangers [25–27]. The injection of air bubbles into the plate heat exchanger resulted in an increase in the number of transfer units (NTU) by up to 12.4% and an enhancement of its effectiveness by up to 14.6%. On the other hand, the entropy increased by up to 4.1 W/K [25]. In a study by Hasan et al. [25], it was found that the size of bubbles had a significant impact on the thermal performance of the heat exchanger. The maximum NTU and effectiveness increased by 153% and 68%, respectively. The bubble injection technique has been shown to enhance NTU and effectiveness by 59% and 18.6%, respectively, on the cold-water side of the heat exchanger [27].

Despite the significance of thermal management in electric vehicle systems, most existing research still focuses on conventional approaches such as model-based control, energy optimization, or mean and threshold-based temperature monitoring [1,6–10], [11–13]. These approaches have been shown to ignore the complex, dynamic characteristics of temperature signals, which are nonlinear and stochastic during real operation.

To date, the utilization of advanced statistical signal analysis technique — particularly Kolmogorov entropy and Probability Density Function (PDF) — has been extremely limited in the context of electric vehicle thermal management. However, it should be noted that these two methods have the capacity to capture deeper insights into chaotic behavior, system complexity, and the probabilistic distribution of temperature fluctuations that conventional statistical parameters alone cannot.

This research gap is of significance because a more comprehensive characterization of temperature signals is directly related to the reliability and durability of thermal control systems. High Kolmogorov entropy can indicate unstable or unpredictable system dynamics, potentially increasing controller workload and accelerating component degradation [28,29]. Conversely, PDFs that exhibit extreme temperature distributions or heavy tails can serve as indicators of the risk of recurring thermal stress. This, in turn, can result in a reduction in system efficiency and shortened lifespan of components such as batteries and thermal actuators [30–32].

The study emphasizes the cooling of controllers with bubble injecton into the colling channel, given the various potentials of bubble cooling in improving thermal performance. Also, the advantages of cooling systems using air and liquid are considered, with the ability to optimize cooling capacity based on the battery thermal load. The study also explores the optimal temperature of the controller, which is greater than the battery. The ejector-type bubble generator, as characterized by Catrawedarma et al. [33], was utilized to inject bubbles into the cooling channel via various air discharges. The impact of the system on thermal performance was evaluated, including the assessment of maximum temperature and thermal resistance during the cooling process. Additionally, the temperature signal was subjected to characterization, including statistical moments, PDFs, and Kolmogorov entropy. Thus, the integration of Kolmogorov entropy analysis and PDFs into the evaluation of thermal management systems offers a more sensitive approach to real-world system dynamics. This study not only fills a gap in the literature but also provides a robust basis for the development of adaptive, robust control strategies oriented towards the enhancement of the energy efficiency and long-term reliability of electric vehicles.

2. Materials and Methods

The present research was conducted at the Mechanical Engineering Workshop, Politeknik Negeri Banyuwangi, with an apparatus schematic as shown in Fig. 1. The primary components in this research include: a battery pack consisting of 24 prismatic 3.2V 30Ah LiFePO4 battery cells connected in series; one unit of the Jikong battery management system (BMS) to regulate the distribution of electricity to all battery cells via 24 pins; and water as the cooling medium. The apparatus comprises a 2000W mid-driven BLDC electric motor acting as a load on the battery, a Nanjing 72360 controller to regulate the electric current to the motor, an aluminium water block as a cooling fluid channel, a 2.4W DC5V water pump to circulate cooling water, a 1.0 W aerator to circulate air, and a bubble generator ejector to form bubbles. The measuring instruments employed in this study include water and air flow meters to measure input air flow. Additionally, a K-type thermocouple was employed to measure the temperature on the controller wall. The study also involved the use of input and output temperatures with a total of 10 thermocouples. Subsequently, the system was installed in accordance to the wiring installation schematic as depicted in Fig. 1(a), the controller cooling system schematic illustrated in Fig. 1(b), and the actual apparatus demonstrated in Fig. 1(c).

The data collection stage begins by filling the cooling water from the water outlet hole to a height of 8 cm within the water-air separator. The subsequent stage of experiment involved activating the water pump to establish a maximum flow rate of 3.4 lpm within the water block, as illustrated in Fig. 1(b). The aerator was activated to facilitate the flow of air into the bubble generator, with the air flow set to a range of 0.1-1.5 lpm. It represents the transition from low to high flow rates, thereby allowing for a clearer understanding of the effects of bubble distribution and thermal interactions of homogeneously distributed bubbles, local turbulence, and diminishing returns due to bubble coalescence, as characterized by [33,34].

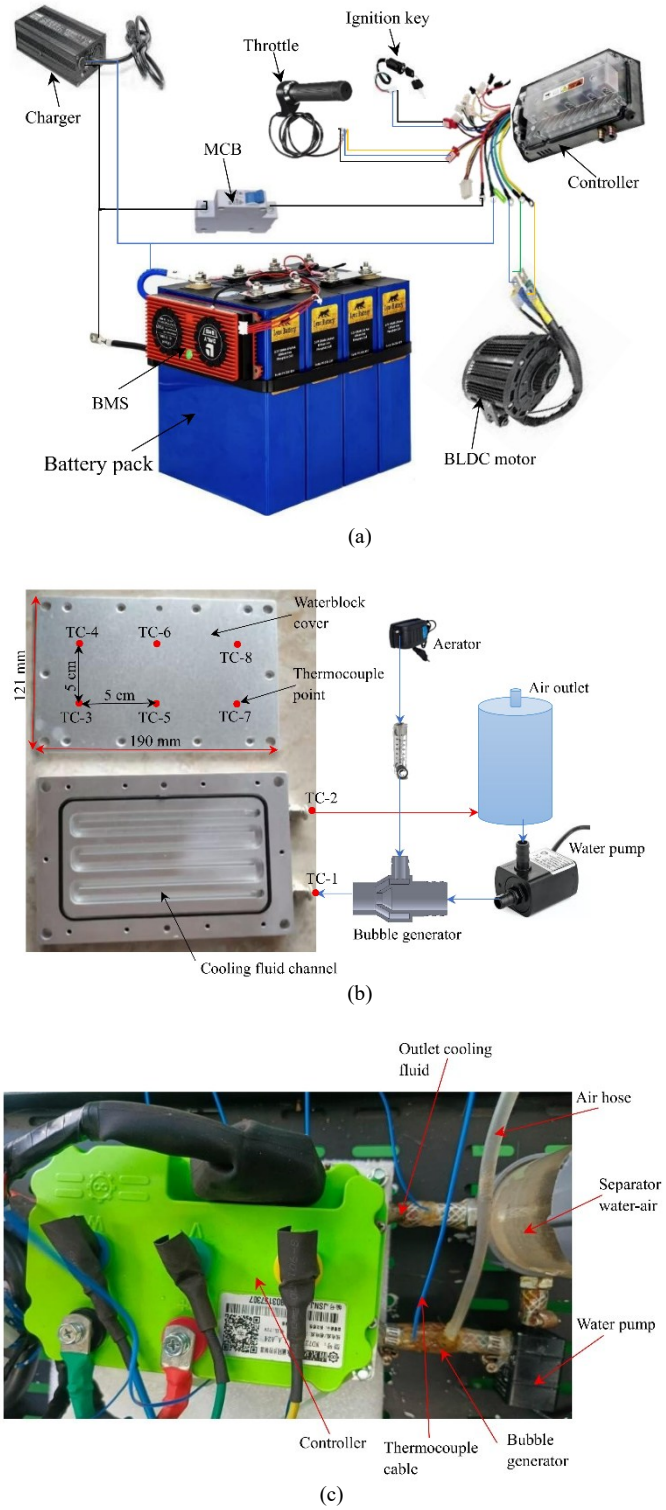

Fig. 1. (a) Schematic wiring diagram of an electric vehicle, (b) Schematic diagram of controller cooling by bubble generator, (c) Real installation of controller cooling by bubble generator

Subsequent to the system's stabilization, a duration of five minutes was observed, after which the temperatures of all controller walls and the input and output temperatures were recorded. The locations of these temperatures are illustrated in Fig. 1(b). The temperature was recorded every 3 seconds using a Lutron BTM-4208SD data logger. Five minutes later, the ignition key was in the ON position, and the electric motor was set to maximum speed by adjusting the throttle. The sequence of process starts by giving the load to the controller. The motor operates for a duration of 30 minutes, followed by a 2.5-hour cooling cycle. Subsequently, the data were processed to obtain the maximum temperature and thermal resistance. The temperature data were the average of three replicate experiments. The average difference was found to be 0.1°C, indicating good repeatability and stability of the experimental system. The thermocouple and input power accuracy levels were found to be 0.4% and 0.3%, respectively. Utilizing the propagation error method, the uncertainty in the thermal resistance calculation was determined to be ±0.00547°C/W.

The ability of a medium to prevent heat transport was measured by its thermal resistance. Convection thermal resistance ($Rcon$) and advection thermal resistance ($Radv$) add up to total thermal resistance (Rt) in fluid cooling [35]. Advection thermal resistance is the result of the fluid's temperature rising due to heat absorption during flow. In contrast, thermal convection resistance is generated from the temperature difference between the cooling fluid and the heated wall.

$$Rcon = \frac{1}{2.A.h} \tag{1}$$

$$A = D_d.L \tag{2}$$

$$h = \frac{k.Nu}{D_h} \tag{3}$$

$$D_h = \frac{2.D_d.D_w}{D_d + D_w} \tag{4}$$

$$Nu = -1.074 + 9.326.G \tag{5}$$

$$G = \frac{\alpha^2 + 1}{(\alpha + 1)^2} \tag{6}$$

$$\alpha = \frac{D_w}{D_d} \tag{7}$$

$$Radv = \frac{1}{Q.\rho_f.C_{pf}} \tag{8}$$

$$Rt = Rcon + Radv \tag{9}$$

where $Rcon$ is the convection thermal resistance, A is the channel area (m^2), h is the heat transfer coefficient, D_d is the height of the channel (m), L is the length of the channel (m), k is the thermal conductivity of the fluid, Nu is the Nusselt number, D_h is the hydraulic diameter, D_w is the width of the channel, Q is the fluid discharge, ρ_f is the fluid density, and C_{pf} is the fluid heat capacity.

3. Results and Discussion

3.1. Temperature time series

Fig. 2(a) presents the time-to-temperature curves of nine thermocouples (TC-1 to TC-9) in a stationary fluid cooler. The vertical axis represents temperature, and the horizontal axis represents time. Each curve represents the reading from a single

thermocouple. The majority of the controller wall temperature curves demonstrate a sharp initial increase, a peak, and an exponential decline. The sharp increase in temperature is observed when the BLDC motor is started at 1800s, as in region (i), and then switched off, resulting in a rapid in temperature as depicted in region (ii). This pattern is common occurrence in thermal transients characterized by rapid-heating, slow-cooling. The exponential decrease in temperature indicates a cooling system dominated by convection. TC-1 and TC-2 are the inlet and outlet temperatures, located somewhat further from the heat source on the controller wall, resulting in a more gradual increase and decrease. The decrease in TC-1 is more gradual than that of TC-2 because TC-2 is the outlet thermocouple, which is closer to the water-air separator, which is open to the atmosphere. TC-9 is an ambient temperature that displays a minimal fluctuation and is accompanied by reference temperature. TC-5 and TC-7 exhibit very high fluctuations during the process of heating. This phenomenon occurs due to the positioning of thermocouples, which are situated in the downstream of the inlet. In this location, the influence of random bubbles and water motion is significant, as well as changes in the two-phase flow momentum. This random movement is caused by the collision, rupture, and merging of bubbles that occur after the inlet. This phenomenon aligns with the observation reported by [36]. The maximum temperatures recorded for TC-3 to TC-8 indicate that the distribution of heat is distributed evenly throughout the controller wall. However, TC-1 and TC-2 exhibit slightly higher maximum temperatures, as evidenced by the lower maximum temperatures recorded in those controllers. It is caused by the cooling water not circulating, resulting in the restriction of heat transfer to solely natural convection.

As illustrated in Fig. 2(b), the temperature distribution on the controller wall and at the inlet and outlet for the circulating coolant. The temperature at the controller wall is denoted by TC-3 to TC-8, the inlet and outlet temperatures by TC-1 to TC-2, and the ambient temperature by TC-9. With the exception of TC-9, all thermocouples exhibited a rapid, uniform temperature rise, indicating even heating. This relatively synchronous rise is due to the uniform distribution of heat. The decline of temperature after the peak is characterized by a slow exponential curve, which indicates natural cooling processes (convection or radiation). It is evident that all TC-1 to TC-8 experience a temperature decline with a nearly identical pattern, indicating even heat distribution, with no outliers or significant differences, as with cooling with quiet water. A comparison of cooling with quiet and circulating water reveals that heat is distributed to the inlet and outlet fluids, resulting in a significantly more even temperature distribution in circulating-water cooling. It is due to the water flow, which also transports heat from the controller wall. These results are consistent with those reported by [37] in a study of microchannel cooling devices.

Fig. 3(a) presents a standard time-series temperature curve for various cooling-fluid conditions, ranging from quiet water to circulating water to bubble cooling with various air flow rates on a single controller walls (TC-7). Quiet water is a standard cooling method that does not involve the flow of water or the formation of bubbles. Under these conditions, the pump and aerator were not activated. The data reveals that, as the temperature is increased 0 to 1800s in region (i), there is a rapid and simultaneous increase in temperature across all curves. It means that all controller walls experience heating with identical thermal treatment. In the case of a BLDC motor in a state of rest, the phenomenon of cooling results in different temperature drops across the thermocouples. The maximum temperature of quiet water is recorded as 49.0 °C, then decreasing significantly to 44.8 °C when the water is in motion, and to 44.1 °C when the bubble is injected at a flow rate of Qa = 0.1 lpm.

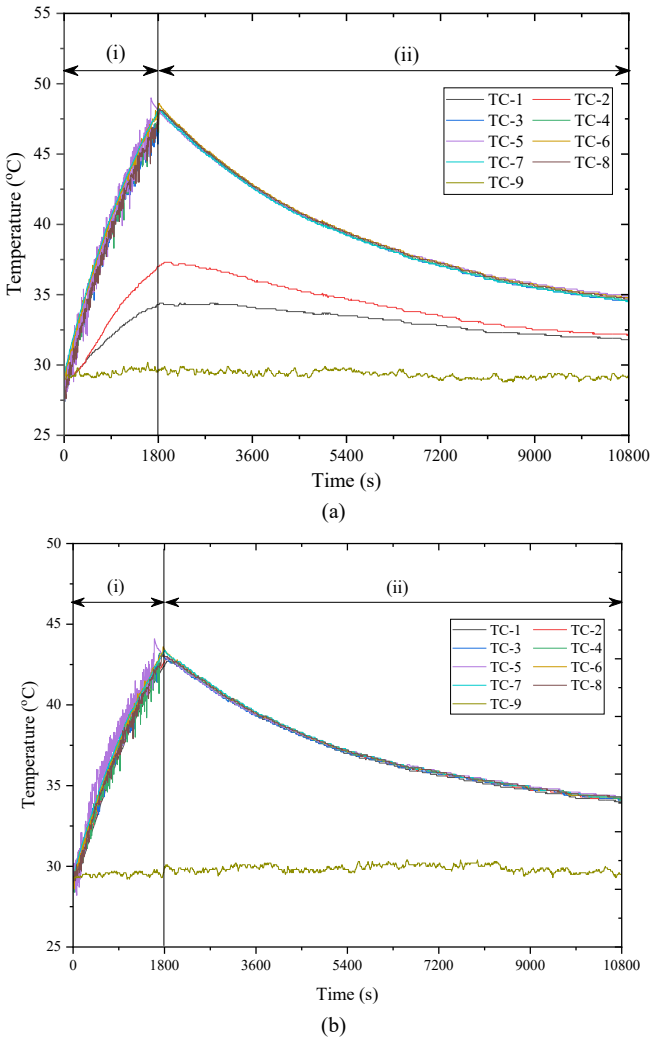

Fig. 2. Temperature of controller for various thermocouple positions at: (a) Quient water, (b) Cooling bubble with Qa = 0.1 lpm

The maximum temperature decrease of 8.57% is observed from cooling with quiet water to cooling with circulating water, and a 15.5% decrease is seen from cooling with quiet water to cooling with bubble injection at an air flow rate of Qa = 1.5 lpm. A 7.59% reduction in the cooling fluid is observed when water is moved to bubble injection at Qa = 1.5 lpm. The findings of the study demonstrate that there is a maximum temperature decrease of 1.38% from the air flow rate Qa = 0.1 lpm to 0.5 lpm and a reduction of 2.1% from the air flow rate Qa = 0.5lpm to to 1.0 lpm. The lowest decrease of 0.95% occurs at air flow rates ranging from Qa = 1.0 to 1.5 lpm. The increase in the injected airflow rate results in a decrease in the maximum temperature. This phenomenon occurs as a result of the interaction between water and air, which forms bubbles in the

channel. The subsequent random flow in the channel is related to the surface tension and buoyancy properties of the bubbles [38,39]. The random flow distribution of heat is a consequence of the fluctuating contact time between the fluid and the controller wall, acting as a heat source. It has been demonstrated that an increase in air flow rate results in an increase in the velocity of the two-phase fluid within the channel, thus leading to a more even heat distribution. Consequently, the cooling mechanism that employs quiet water has the slowest cooling rate because it relies on natural convection. The presence of circulating coolant has been demonstrated to accelerate cooling process through the enhancement of heat transfer via forced convection [40]. The process of adding air to form bubbles accelerates cooling. Increasing the airflow rate accelerates heat distribution, thereby demonstrating that forced convection can enhance heat transfer[41].

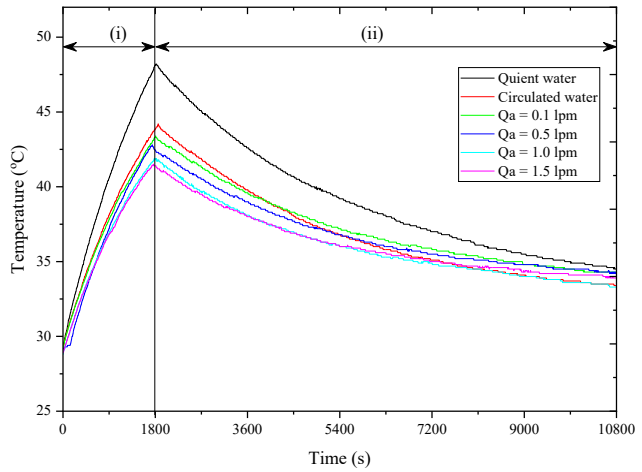

Fig. 3. (a) Temperature of the controller for various flow rates at TC-7, (b) Temperature at the outlet of the water block (TC-2) for various flow rates

Fig. 3(b) depicts the temperature change at the outlet (TC-2). The measured temperature is the coolant fluid leaving the water block. This phenomenon provides further evidence to support the conclusion that the quiet-water coolant fluid is not able to distribute temperature optimally. It is evident from the outlet temperature, which is lower than the temperature of circulating fluid. The outlet temperature of the circulating fluid is close to the maximum temperature, as demonstrated in Fig. 3(a). The outlet temperature of the quient water is 37 °C, which is significantly lower than the maximum temperature of the controller wall of 48.2 °C. The outlet temperature is measured at 43.7 °C during water circulation, and subsequently decreases to 42.9 °C, 42.3 °C, 41.7 °C, and 41 °C at input air flow rates of Qa = 0.1 lpm, 0.5 lpm, 1.0 lpm, and 1.5 lpm, respectively. The maximum outlet temperature is 0.44 °C lower than the controller wall's maximum temperature. The phenomenon is caused by the influence of the controller wall thickness, the distance between TC-7 and TC-2, and the position of TC-2, which is closer to the water-air separator open to the atmosphere. This results in TC-2's temperature decreasing more quickly.

3.2. Resistensi thermal

Thermal resistance is defined as the resistance to heat flow through a medium interface. Its occurrence is observed at the interface of solid-liquid, liquid-gas, or liquid-liquid media. The presence of high thermal resistance results in the obstruction of heat flow, while low thermal resistance facilitates unobstructed heat flow. In cooling using a water block for flowing fluids, there are two types of thermal resistance: convection and advection [35]. Fig. 4(a) depicts the convection thermal resistance during cooling with only flowing water, and with flowing water plus air injection at 0.1 lpm, 0.5 lpm, 1.0 lpm, and 1.5 lpm, respectively. The trend exhibited in this graph is that an increase in the injected airflow rate is associated with the increase in convection thermal resistance. The findings demonstrate the correlation between the airflow rate and the size and the number of the formed bubbles, with greater buoyancy [32]. It has been demonstrated that the objects under consideration occupy positions above the channel and tend to increase the thermal contact resistance. It makes it more challenging to make contact between the cooling water and the controller wall. The convection thermal resistance of circulating water is slightly higher than that of air injection with a flow rate of Qa = 0.1 lpm. This is because at this flow rate, the dominant formation is of bubbles with a low diameter, high surface tension, low rising velocity, and low buoyancy. These bubble are able to mix evenly with water, thereby increasing the convection heat transfer coefficient[41].

Fig. 4(b) depicts the advection thermal resistance, which is defined as heat transfer as result of the movement of fluid mass that carries heat. It has been demonstrated that an increase in the injected air flow rate results in a decrease in advection thermal resistance. As the air flow rate is increased, the two-phase air-water flow rate is accordingly elevated and thus the the fluid velocity is increased. In addition, an increase in airflow rate results in an increase in the number of bubbles formed, with larger diameters. Furthermore, an increase in buoyancy results in an increase in bubble velocity, thereby increasing the two-phase velocity [34,36,42]. As a consequence, the greater the fluid mass movement, which also carries heat, the greater the advection heat transfer. Fig. 4(c) depicts the total thermal resistance, representing the sum of the convection and advection thermal resistances. As seen in the figure, the advection thermal resistance has a dominant

influence on the total thermal resistance, as indicated by the trend of the diagram.

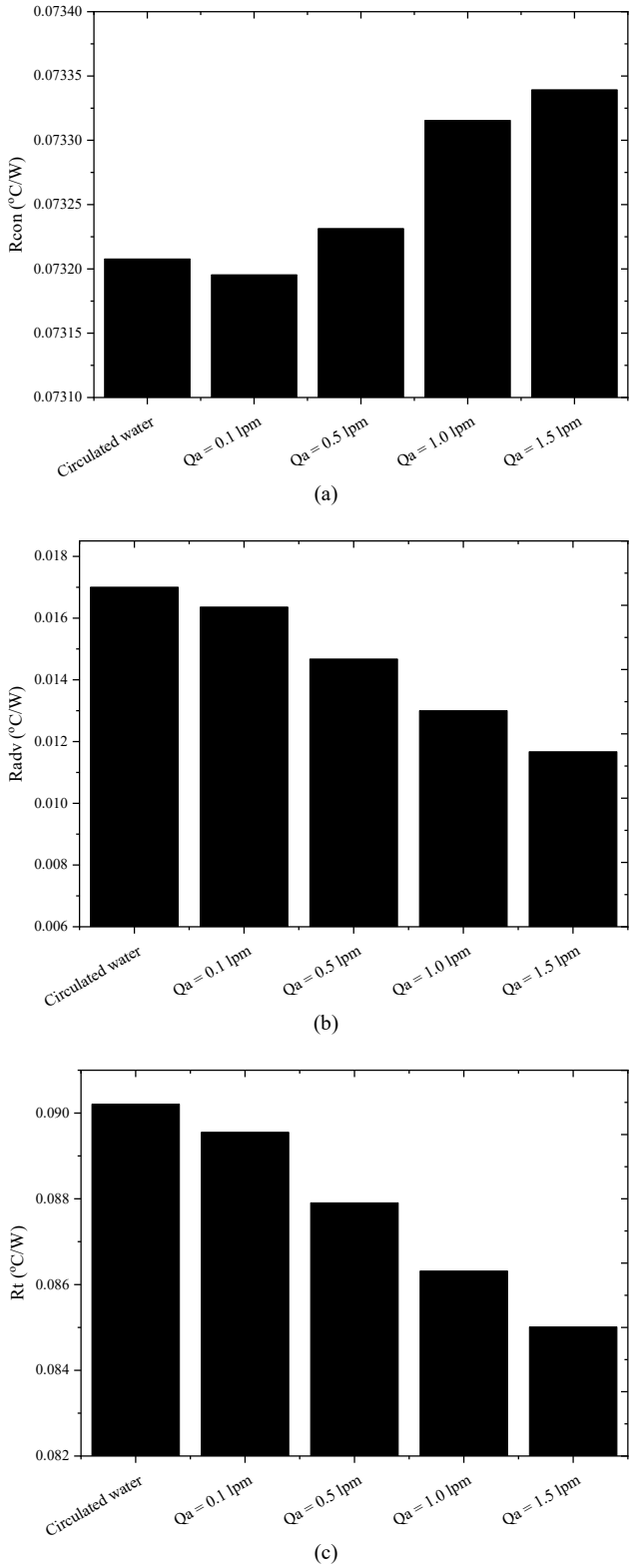

Fig. 4. (a) Convection thermal resistance, (b) Advection thermal resistance, (c) Total thermal resistance

At high gas flow rates, the distribution of bubble becomes increasingly inhomogeneous due to the effects of buoyancy and interactions between bubble. This leads to the accumulation of bubbles near the top wall or in specific regions of the channel [43]. This accumulation increases the local void fraction and forms a partial gas layer that acts as a thermal barrier, thus increasing the thermal contact resistance between the liquid fluid and the solid surface.

Furthermore, studies of bubble-surface interactions have demonstrated that bubbles have the capacity to adhere, rebound, or form interfacial layers that interfere with local heat transfer [44]. In certain conditions, this phenomenon has been observed to reduce the effectiveness of local convection even as the flow rate increases. However, an increase in the airflow rate still reduces the system's total thermal resistance. This phenomenon is related to the dominance of advection mechanisms and bubble-induced fluid agitation, which significantly enhance mixing and heat transport [45]. It is recognized that bubbly flow is capable of substantially increasing turbulence and velocity fluctuations, thereby enhancing volumetric heat transfer despite local degradation in certain areas [46].

Consequently, the observed phenomenon can be interpreted as a competition between two mechanisms: (i) an increase in local resistance due to the accumulation of bubbles and the formation of gas layer, and (ii) an increase in global heat transfer due to advection and turbulence enhanced by the two-phase flow. The dominance of the second mechanism at higher flow rates explains why the total thermal resistance remains decreased despite the increase in local convection resistance.

3.3. Stochastic parameter

Fig. 5 illustrates the probability density function of the temperature time series. It can be seen that the quiet water cooling fluid at the input (TC-1) and output (TC-2) exhibits a temperature distribution with the highest flatness. This finding indicates that the temperature distribution range is relatively linited due to the influence of natural convection heat transfer, which has a low heat transfer rate. Consequently, heat from the controller is not immediately distributed to the input and output. TC-3 to TC-8 are parts in direct contact with the controller, thus resulting in a longer temperature distribution and smaller flatness. The mean PDF reveals that the majority of temperatures are distributed around 35 °C, indicating that this temperature has the highest frequency of occurrence.

Fig. 6(a) displays the maximum temperature of all thermocouple positions and all variations in air flow. The secondary Y-axis is designated for quiet-water fluid, which exhibits a higher maximum temperature than the other positions on the controller wall. The maximum temperature of quiet water at positions TC-1 and TC-2 is relatively low because it measures the inlet and outlet temperatures of the water block. These temperature are somewhat far from the controller wall and closer to the open separator. The movement of the cooling fluid results in a greater airflow, and thus a lower the maximum temperature of the controller wall [37]. This finding suggests that heat can be distributed more effectively at higher airflow. This phenomenon is related to an increase in the flow momentum, which in turn raises the Reynolds number and, eventually, the heat transfer coefficient by convection. The maximum temperature is observed at positions TC-5 and TC-6, indicating that it is in the center of the controller.

Fig. 6(b) depicts the average temperature for all coolant-fluid and thermocouple-position combinations. The trend is

similar to the maximum temperature, yet the average temperature at Qa = 0.1 lpm is higher than that of the circulating water. This occurrence is related to slightly higher temperature during cooling in comparison to the circulating water, due to smaller-diameter bubbles with greater surface tension, thereby reducing heat dissipation [41].

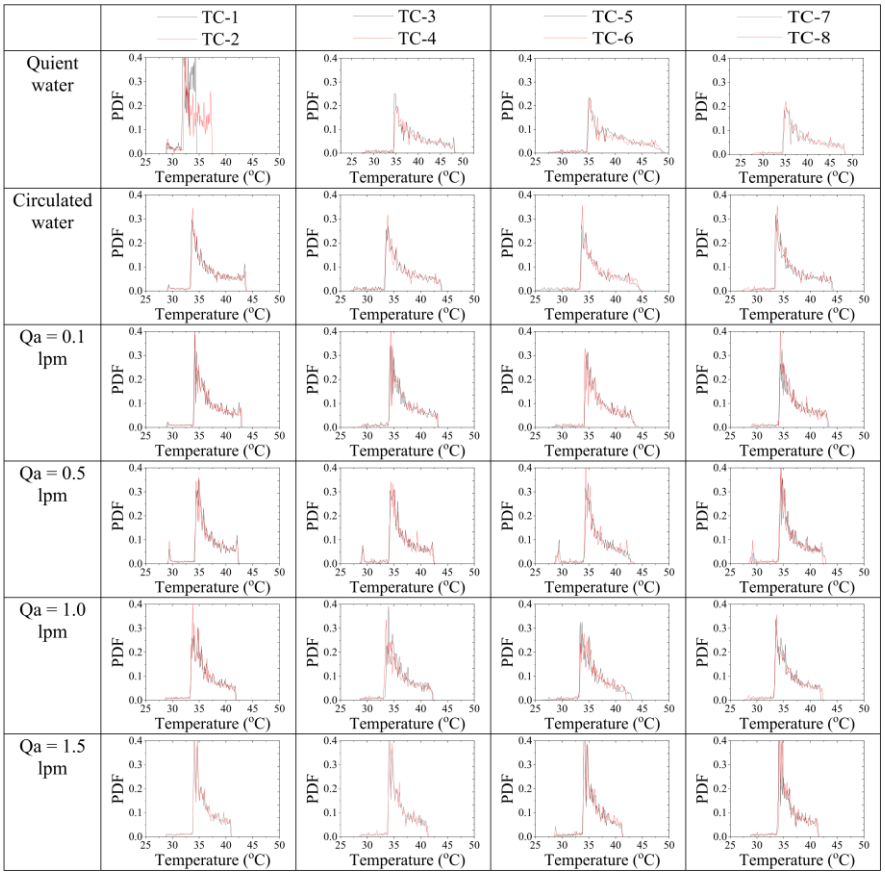

Fig. 5. Probability density function

As illustrated in Fig. 6(c), the temperature variance is utilized as an indicator of the amplitude of the temperature signal[38,47]. Amplitude refers to the amount of energy carried by a signal or the intensity of a signal. In the case of the quiet water, the amplitude tends to be higher, indicating the increase of the signal intensity in view of the absence of random movement to enhance heat dissipation[48]. As the airflow rate increases, the flow in the cooling channel becomes heterogeneous, potentially increasing heat transfer. The implication is that the signal intensity becomes lower. In such condition, advection heat transfer is more dominant in determining the signal intensity.

Fig. 6(d) and (e) demonstrate the tendency of skewness and flatness to be inversely related. Skewness refers to the symmetry of the PDF curve relative to its mean value, and flatness is defined as the degree of sharpness of a curve. It is evident that an increase in air flow rate results in an increase in skewness and a decrease in flatness. It indicates that the greater the skewness, the narrower the temperature distribution, thereby increasing the likelihood of its occurrence, which in turn increases the PDF. It is also shown that a decrease in flatness lead to an increase in temperature distribution, as indicated by a decline in the PDF. Quiet water exhibits the highest skewness, indicating that the PDF is more left-skewed, indicating that the majority of of the data is distributed to the left of the mean. A negative skewness value, such as at Qa = 0.5 lpm, indicates that the majority of the temperatures are to the right of the mean.

Furthermore, high skewness indicates an asymmetric temperature distribution, which indicates a tendency for the controller to experience momentary temperature spikes (thermal spikes). This condition can increase the non-uniformity of heat distribution in electronic components, thereby accelerating material degradation from repeated thermal expansion-contraction cycles [49–51]. Conversely, a high flatness indicates a greater probability of extreme temperature fluctuations in comparison to a standard Gaussian distribution. In an engineering context, this condition indicates an increased risk of thermal overstress in the control module. This can accelerate sensor performance degradation, increase temperature measurement errors, and ultimately reduce the reliability of the thermal management system [30–32].

Fig. 7 illustrates the Kolmogorov entropy as an indicator of a signal's irregularity. It is evident that the more periodic the temperature signal, the smaller the entropy. Of all variables, entropy in quiet water tends to be lowest because heat transfer is relatively slow, leading to a periodic pattern of temperature changes. It has been demonstrated that circulating water and cooling fluid with Qa = 0.1 lpm exhibit the highest entropy. This is due to the fact that, with low airflow, the bubbles formed are smaller, increasing the likelihood of collision, rupture, and merging. The increase in hydrodynamic forces leads to a more

diverse temperature fluctuation pattern, which, in turn, increases entropy. The entropy of the cooling fluid with air flow (Qa = 1.5 lpm) exhibits a relatively even distribution across all thermocouple positions. This finding indicates that the temperature fluctuation pattern tends to remain constant, with a more even temperature distribution due to increasing flow velocity. Consequently, this leads to an increase in the Reynolds number and, in turn, the convection heat transfer coefficient. The entropy at TC-5 for the cooling fluid with Qa = 0.5 lpm and Qa = 1.0 lpm is the highest among the other thermocouple positions. This phenomenon is related to the influence of the hydrodynamic entrance length when the air-water mixture begins to enter the cooling channel, which has not yet fully developed.

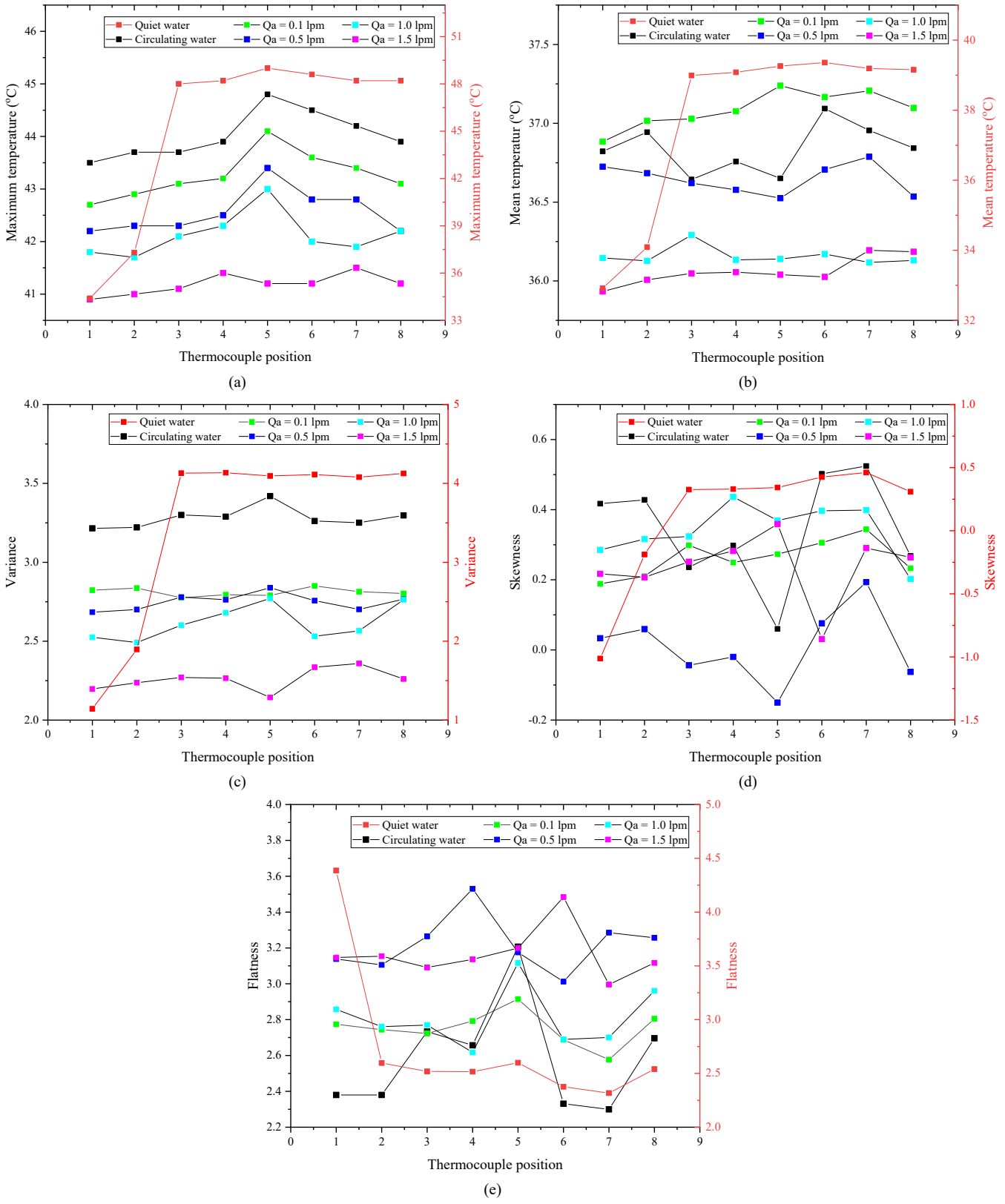

Fig. 6. Statistical moment: (a) Maximum temperature, (b) Mean temperature, (c) Variance, (d) Skewness, (e) Flatness

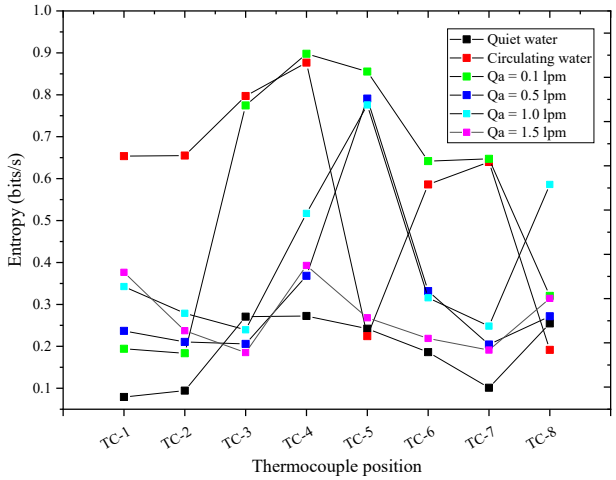

Fig. 7. Kolmogorov entropy for all thermocouple positions and various air flow rates

Furthermore, high Kolmogorov entropy indicates greater complexity of temperature dynamics and lower signal predictability. This observation signifies that the system experiences thermal fluctuations that are challenging to predict with conventional control algorithms. From an implementation perspective, this condition requires more adaptive or robust control strategies, such as model predictive control or learning-based algorithms, to ensure the maintenance of optimal system response to thermal disturbances [28,29].

4. Conclusion

A study was conducted to examine the changes of temperature during the heating and cooling process of an electric vehicle controller utilizing a bubble generator-based cooling mechanism at various thermocouple positions and variations in the input air flow rate. The temperature time series data were analyzed to obtain the maximum temperature, thermal resistance, PDF, and Kolmogorov entropy. Concurrently, statistical parameters such as mean, variance, skewness, and flatness were utilized to characterize the PDF. The results indicated that cooling with circulating water produced a more even temperature distribution compared to cooling with quiet water. It is demonstrated that increasing the injected air flow rate led to a reduction in the maximum temperature when using bubbles as a cooling medium at Qa = 1.5 lpm, by 15.5% in comparison to quiet water.

On the other hand, an increase in the airflow rate resulted in an enhancement of the convection thermal resistance. In contrast, the advection thermal resistance tended to decrease, therebybproviding a dominant contribution to the total thermal resistance. The PDF indicates that the majority of the temperature distribution is approximately 35°C. However, an increase in the airflow rate results in higher skewness and lower flatness, indicating wider, less symmetrical temperature fluctuations. In addition, quiet water conditions exhibits the lowest Kolmogorov entropy, while cooling with an airflow rate of Qa = 1.5 lpm results in a relatively uniform entropy distribution across all thermocouple positions, indicating enhanced thermal dynamic stability at the controller surface.

To facilitate further research, it is pivotal to address the following limitations of the current research: firstly, the parameter range needs to be expanded by including more realistic dynamic load scenarios that reflects real conditions to increase practitioner relevance. Secondly, statistical analysis must be integrated with physics-based models or data-driven approaches such as machine learning to enhance the predictive capabilities of the research, and thirdly, the direct relationship between statistical parameters (e.g., entropy and flatness) and indicators of degradation, reliability, and system lifetime must be explored quantitatively.

Acknowledgements

This research constitutes a small part of the ejector bubble generator application research conducted in the Multiphase Flow Research Group of Banyuwangi State Polytechnic, Indonesia. The authors would like to express their gratitude to Deqi Pajar Pratama, Rizqi Novan Wijaya, and M. Yatim for their assistance in manufacturing the apparatus. IGNB. Catrawedarma also expressed his gratitude to Politeknik Negeri Banyuwangi, through the Center for Research and Community Service, for financial support under the Penelitian Berbasis Rencana Induk Penelitian (PBRIP) scheme, contract number 5781.5/PL36/AL.04/2025.

References

1. S. Hekmat, G.R. Molaeimanesh, Hybrid thermal management of a Li-ion battery module with phase change material and cooling water pipes: An experimental investigation, Applied Thermal Engineering. 166 (2020) 114759.
2. A.A. Pesaran, Battery Thermal Management in EVs and HEVs: Issues and Solutions, Advanced Automotive Battery Conference. (2001).
3. J. Kim, J. Oh, H. Lee, Review on battery thermal management system for electric vehicles, Applied Thermal Engineering. 149 (2019) 192–212.
4. J.-M. Mottard, C. Hannay, E.L. Winandy, Experimental study of the thermal behavior of a water cooled Ni–Cd battery, Journal of Power Sources. 117 (2003) 212–222.
5. A. Kumar Thakur, R. Sathyamurthy, R. Velraj, R. Saidur, A.K. Pandey, Z. Ma, P. Singh, S.K. Hazra, S. Wafa Sharshir, R. Prabakaran, S.C. Kim, S. Panchal, H.M. Ali, A state-of-the art review on advancing battery thermal management systems for fast-charging, Applied Thermal Engineering. 226 (2023) 120303.
6. Q. Huang, X. Li, G. Zhang, J. Zhang, F. He, Y. Li, Experimental investigation of the thermal performance of heat pipe assisted phase change material for battery thermal management system, Applied Thermal Engineering. 141 (2018) 1092–1100.
7. M. Mahmud, K.S. Rahman, Md. Rokonuzzaman, A.K.M.A. Habib, M.R. Islam, S.M.A. Motakabber, S. Channumsin, S. Chowdhury, Lithium-ion battery thermal management for electric vehicles using phase change material: A review, Results in Engineering. 20 (2023) 101424.
8. L. Ianniciello, P.H. Biwolé, P. Achard, Electric vehicles batteries thermal management systems employing phase change materials, Journal of Power Sources. 378 (2018) 383–403.
9. J. Weng, D. Ouyang, X. Yang, M. Chen, G. Zhang, J. Wang, Optimization of the internal fin in a phase-change-material module for battery thermal management, Applied Thermal Engineering. 167 (2020) 114698.

10. Z. Rao, S. Wang, G. Zhang, Simulation and experiment of thermal energy management with phase change material for ageing LiFePO4 power battery, Energy Conversion and Management. 52 (2011) 3408–3414.
11. S.A. Khateeb, S. Amiruddin, M. Farid, J.R. Selman, S. Al-Hallaj, Thermal management of Li-ion battery with phase change material for electric scooters: experimental validation, Journal of Power Sources. 142 (2005) 345–353.
12. S.A. Khateeb, M.M. Farid, J.R. Selman, S. Al-Hallaj, Design and simulation of a lithium-ion battery with a phase change material thermal management system for an electric scooter, Journal of Power Sources. 128 (2004) 292–307.
13. A. Hussain, Thermal management of lithium ion batteries using graphene coated nickel foam saturated with phase change materials, International Journal of Thermal Sciences. (2018).
14. C. Wang, Heat transfer enhancement of phase change composite material: Copper foam/paraffin, Renewable Energy. (2016).
15. P. Goli, S. Legedza, A. Dhar, R. Salgado, J. Renteria, A.A. Balandin, Graphene-Enhanced Hybrid Phase Change Materials for Thermal Management of Li-Ion Batteries, Journal of Power Sources. (2013).
16. C. Lin, Experiment and simulation of a LiFePO4 battery pack with a passive thermal management system using composite phase change material and graphite sheets, Journal of Power Sources. (2015).
17. Z. Ling, Experimental and numerical investigation of the application of phase change materials in a simulative power batteries thermal management system, Applied Energy. (2014).
18. Z. Ling, Thermal management performance of phase change materials with different thermal conductivities for Li-ion battery packs operated at low temperatures, (2018).
19. F.S. Hwang, T. Confrey, C. Reidy, D. Picovici, D. Callaghan, D. Culliton, C. Nolan, Review of battery thermal management systems in electric vehicles, Renewable and Sustainable Energy Reviews. 192 (2024) 114171.
20. N. Putra, B. Ariantara, R.A. Pamungkas, Experimental investigation on performance of lithium-ion battery thermal management system using flat plate loop heat pipe for electric vehicle application, Applied Thermal Engineering. 99 (2016) 784–789.
21. R. Sukarno, Z. Indasyach Moreno, D. Rio Budi Syaka, Y. Gunawan, N. Gama Yoga, R. Fariz Adzani, A. Putra Mustafit, D. Kurniawati, Experimental investigation of a thermoelectric generator assisted with heat pipe sinks for pickup car exhaust waste heat recovery, CST. 10 (2025) 106–116.
22. Y. Ye, Y. Shi, L.H. Saw, A.A.O. Tay, Performance assessment and optimization of a heat pipe thermal management system for fast charging lithium ion battery packs, International Journal of Heat and Mass Transfer. 92 (2016) 893–903.
23. J. Smith, R. Singh, M. Hinterberger, M. Mochizuki, Battery thermal management system for electric vehicle using heat pipes, International Journal of Thermal Sciences. 134 (2018) 517–529.
24. C. Roe, X. Feng, G. White, R. Li, H. Wang, X. Rui, C. Li, F. Zhang, V. Null, M. Parkes, Y. Patel, Y. Wang, H. Wang, M. Ouyang, G. Offer, B. Wu, Immersion cooling for lithium-ion batteries – A review, Journal of Power Sources. 525 (2022) 231094.
25. Z.M. Marouf, M.A. Fouad, M.A. Hassan, Experimental investigation of the effect of air bubbles injection on the performance of a plate heat exchanger, Applied Thermal Engineering. 217 (2022) 119264.
26. S. S. Hasan, A. Sh. Baqir, H. B. Mahood, The Effect of Injected Air Bubble Size on the Thermal Performance of a Vertical Shell and Helical Coiled Tube Heat Exchanger, Energy Engineering. 118 (2021) 1595–1609.
27. Z.M. Marouf, M.A. Fouad, Combined Energetic and Exergetic Performance Analysis of Air Bubbles Injection into a Plate Heat Exchanger: An Experimental Study, Energies. 16 (2023) 1164.
28. F. Colonius, C. Kawan, Invariance Entropy for Control Systems, SIAM J. Control Optim. 48 (2009) 1701–1721.
29. H. Jin, Y. Guan, L. Yao, Minimum Entropy Active Fault Tolerant Control of the Non-Gaussian Stochastic Distribution System Subjected to Mean Constraint, Entropy. 19 (2017) 218.
30. M. Bröcker, L. Herrmann, Flatness based control and tracking control based on nonlinearity measures, IFAC-PapersOnLine. 50 (2017) 8250–8255.
31. H. Gharsallaoui, M. Ayadi, M. Benrejeb, P. Borne, Flatness-based Control and Conventional RST Polynomial Control of a Thermal Process, INT J COMPUT COMMUN. 4 (2009) 41.
32. S. Scholz, L. Berger, D. Lebiedz, Benchmarking of Flatness-based Control of the Heat Equation, (2023).
33. I. Catrawedarma, S. Ton, D.D. Pranowo, F. Surahmanto, Size Distribution and Mean Diameter of Microbubbles in Different Types of Ejector Bubble Generators, JAFM. 18 (2025).
34. I. Catrawedarma, S. Ton, D.D. Pranowo, F. Surahmanto, Hydrodynamic characteristics of the microbubble dissolution in water using an ejector-type bubble generator, Case Studies in Chemical and Environmental Engineering. 11 (2025) 101043.
35. H. Park, A design of air flow configuration for cooling lithium ion battery in hybrid electric vehicles, Journal of Power Sources. 239 (2013) 30–36.
36. E.N. Sari, A. Fiveriati, N. Rusti, J. Rulianto, R. Bhiqman Susanto, I. Catrawedarma, Visual and Pressure Signal Investigations on Bubble Produced by Ejector Bubble Generator, E3S Web Conf. 483 (2024) 03020.
37. S. Riera, J. Barrau, M. Omri, L.G. Fréchette, J.I. Rosell, Stepwise varying width microchannel cooling device for uniform wall temperature: Experimental and numerical study, Applied Thermal Engineering. 78 (2015) 30–38.
38. I. Catrawedarma, D. Deendarlianto, I. Indarto, Statistical Characterization of Flow Structure of Air–water Two-phase Flow in Airlift Pump–Bubble Generator System, International Journal of Multiphase Flow. 138 (2021).
39. I. Catrawedarma, Deendarlianto, Indarto, Hydrodynamic behaviors of air–water two-phase flow during the water lifting in a bubble generator type of airlift pump system, Heat and Mass Transfer. 58 (2022) 1005–1026.
40. C. Roy, P. Venuvanalingam, J.F. Klausner, R. Mei, ON THE MECHANISM OF BUBBLE INDUCED FORCED CONVECTIVE HEAT TRANSFER ENHANCEMENT, Frontiers in Heat and Mass Transfer. 11 (2018).
41. A. Kitagawa, Y. Murai, Natural convection heat transfer from a vertical heated plate in water with microbubble injection, Chemical Engineering Science. 99 (2013) 215–224.
42. D.I. Mawarni, W.E. Juwana, I. Catrawedarma, K.A. Yuana, W. Budhijanto, D. Deendarlianto, I. Indarto, Statistical Characterization of Bubble Breakup Flow Structures in Swirl-Type Bubble Generator Systems, ASEAN J. Chem. Eng. 23 (2023) 62.
43. M. Lopez De Bertodano, R.T. Lahey, O.C. Jones, Phase distribution in bubbly two-phase flow in vertical ducts, International Journal of Multiphase Flow. 20 (1994) 805–818.
44. D.B. Donoghue, A. Albadawi, Y.M.C. Delauré, A.J. Robinson, D.B. Murray, Bubble impingement and the mechanisms of heat transfer, International Journal of Heat and Mass Transfer. 71 (2014) 439–450.
45. N.S. Panicker, A. Passalacqua, R.O. Fox, Computational Study of the Effect of Homogeneous and Heterogeneous Bubbly Flows on Bulk Gas–Liquid Heat Transfer, Journal of Fluids Engineering. 142 (2020) 101402.

46. I. Michiyoshi, A. Serizawa, Turbulence in two-phase bubbly flow, Nuclear Engineering and Design. 95 (1986) 253–267.
47. A.H. Astyanto, J.A.E. Pramono, I. Catrawedarma, Deendarlianto, Indarto, Statistical characterization of liquid film fluctuations during gas-liquid two-phase counter-current flow in a 1/30 scaled-down test facility of a pressurized water reactor (PWR) hot leg, Annals of Nuclear Energy. 172 (2022) 109065.
48. U.C. Saxena, A.D.K. Laird, Heat Transfer from a Cylinder Oscillating in a Cross-Flow, Journal of Heat Transfer. 100 (1978) 684–689.
49. J.W.C. De Vries, M.Y. Jansen, W.D. Van Driel, On the difference between thermal cycling and thermal shock testing for board level reliability of soldered interconnections, Microelectronics Reliability. 47 (2007) 444–449.
50. V. Lakshminarayanan, N. Sriraam, The effect of temperature on the reliability of electronic components, in: 2014 IEEE International Conference on Electronics, Computing and Communication Technologies (CONECCT), IEEE, Bangalore, India, 2014: pp. 1–6.
51. S. Moreau, L. Lequeu, R. Jerisian, Comparative study of thermal cycling and thermal shocks tests on 2004, Microelectronics Reliability. 44 (2004) 1343–1347.